Different cold spray deposition strategies : single- and multi-layers to repair aluminium alloy components

Rech, Silvano; Trentin, Andrea; Vezzù, Simone; Vedelago, Enrico; Legoux, Jean-Gabriel; Irissou, Éric

National Research Council Canada   Conseil national de recherches Canada

Canada

Different cold spray deposition strategies: single and multi layers, to repair aluminium alloy component

Silvano Rech, Andrea Trentin, Simone Vezzù, Enrico Vedelago, Veneto Nanotech, Via delle Industrie 12, Marghera, 30175, Italy

Jean-Gabriel Legoux, Eric Irissou, Industrial Materials Institute (IMI), National Research Council Canada (CNRC-NRC), 75 de Mortagne Boulevard, Boucherville, QC J4B 6Y4, Canada

Cold spray is be used on an increased basis in the reconstruction or repair of damaged aluminium alloy components, especially in the aviation industry. Both thin (<0.5 mm) and thick (up to centimeter) coatings are necessary in order to achieve dimensional recovery of the components. Thin and above all thick coatings can be deposited using a *singlepass* (single layer) or with *multipass* (layer upon layer) giving different thermal and stress contribution to the components and coatings itself. The thermal input, the amount and type of residual stresses and porosity impart different characteristics to adhesion, crack propagation and mechanical properties of the coating. In this study two set, single and multipass aluminium alloy (AA6061) coatings of different thickness (from 0.5mm up to 2mm) are deposited on to AA6061 substrates and compared by metallographic and fractographic analysis, fourpoint bending test, residual stress analysis and the Vickers microhardness identation. Finally the coating adhesion and cohesion are measured by standard ASTM-C633 adhesion test and Tubular-Coating-Tensile test. The study demonstrates that none of the two deposition strategies: singlelayer and multilayer is preferable a priori, the choice must be related to the desired property for component restoration.

1 Introduction

Military rotorcraft transmission housings, gear boxes of military and civil aircrafts, made of magnesium or aluminium alloys, and polymer injection moulds made from aluminium alloys can be affected by construction defects (casting defect, porosity) or damage during the service (erosion and abrasion). These defects could be restored by cold spray (Ref 1-3). The cold spray repair process has been demonstrated to be economically advantageous (Ref 4) and it can be incorporated in a repair facility or as part of a production (Ref 5).

Welding (Ref 6) and lasers (Ref 7) are widely used for components restorations, but thermal residual stress and deformation that result from the solidification of the melted material caused by a high thermal input (Ref 8) can degrade the quality of the repaired part (Ref 9), which gives rise to a short lifecycle of the (low-melting magnesium or aluminium alloys) restored components. Cold sprayed aluminium coatings have low compressive residual stress (Ref 10), very low thermal input and no microstructural change (Ref 11). These properties make the cold spray a competitive technology for repair not only in terms of cost and industrialization but also in terms of performance on repaired components.

In a previous work (Ref 12), the presence of tensile stress peaks at interfaces between sequential layers of a multilayer coating was identified and was the motivation to investigate whether other mechanical and structural coating properties could vary with the

deposition strategy in particular with the number layers for the same coating thickness. Therefore the present study is a continuation of the previous study and focuses on the evaluation of the microstructural and mechanical properties of cold sprayed aluminium alloy (AA6061) coatings, deposited on the same alloy substrates, following two different strategies of deposition: *singlepass* (single layer) or *multipass* (layer upon layer). In addition, coatings exhibiting different thicknesses obtained by one single spray pass were investigated to understand how thickness influences coating properties.

The two methodologies were both valid alternatives in achieving high coatings thickness, so it is important to know the structural properties and requirements of the respective coatings in order to perform a restoration suitable to the particular damaged component.

2   Experimental Procedure

The powder sprayed in this study was gas atomized aluminium alloy 6061 (magnesium-silicon aluminium alloy) with particle size ranging between 5 and 50 µm (TLS Technik GmbH, KG, D-06733 Bitterfeld, Germany). The powder ICP analysis provided by the supplier is reported on **Table 1**. The depositions were carried out by means of Cold Spray system (CGT-Kinetiks 3000, CGT Cold Gas Technology GmbH, Ampfing, Germany). A special polymeric nozzle designed for aluminium powder spraying was used. The coatings were deposited on different geometries of AA6061-O aluminium alloy substrates: *plate* (laminated 50x500x4 mm^3) for spray optimizations and metallographic analysis; *4-point* strips (laminated 76x19x2 mm^3) to perform four-point bending test; cylindrical samples (25 mm diameter) to perform *adhesion* and *cohesion* test by ASTM C633 standard and the Tubular Coating Tensile (TCT) test and square plate (25.4x25.4x4 mm^3) to measure residual stress by Modified Layer Removal Method (*MLRM*). The surfaces of the samples were grit blasted with angular corundum (16MESH) in order to optimize the coating adhesion. The average surface roughness was Ra = 14.65±6.63 µm determined by measuring one representative sample for all different geometry substrates.

2.1 Cold Spray Deposition

The main spray parameters were maintained constant for all deposition sets: the stagnation gas temperature was 350 °C and the nitrogen stagnation gas pressure was kept constant at 3.1 MPa. The distance between the nozzle and the substrate was 20 mm (**Fig. 1a**), and the nozzle scan spacing was 1 mm (**Fig. 1b**); the powder flow and carrier gas flow rates (Ref 11) were the same for all depositions. The cold spray gun followed a "Zig-Zag" pattern on the aluminium substrates and each subsequent pass was a repetition of the first pass. In particular for the 4-point strips the pattern was the equivalent of the layout reported in **Fig. 1b**. For all different substrate geometries: plate, 4-point, adhesion, cohesion and MLRM, seven sets of three samples (4 for adhesion) were deposited. In the first four sets (1 to 4) the coating (desired) thickness was varied (respectively: 0.5, 1.0, 1.5 and 2.0 mm) in a singlepass deposition; in the three sets (5 to 7) the coating thickness (2 mm) was kept constant and the number of pass varied (respectively: 2, 3, and 4). There was no time delay between subsequent pass in multilayers coatings. The desiderate thickness was obtained varying the gun traverse speed, and in the case of cohesion substrates, the rotation speed of the cylindrical samples was varied to obtain coating uniformity and thickness. The coating thickness reported for every set is the average of 3 gauge measurements for each sample of the set (total of 9 measurements). A standard deviation is also reported. Process setup and coating thickness of the different samples are summarized in **Table 2** and **Table 3**.

2.2 Metallographic Sample Preparation

The coating microstructure (plate samples: see **Table 3**) was investigated by means of cross-section light optical microscopy (LOM, model DM6000M, Leica, Wetzlar, Germany). All the samples were sectioned and mounted. Grinding was performed using different grades of abrasive papers and a final polish using 1 μm diamond suspensions. Samples were also chemically etched using modified Keller's reagent (2.5 ml NHO_3, 1.0 ml HCl, 1.5 ml HF and 95 ml water).

2.3 Image Analysis

The areal porosity percentage in the coating was measured by image analysis. The LOM coating micrographs (plate samples: see **Table 3**) were processed by SPIP (Scanning Probe Image Processing, Image Metrology A/S, Hørsholm, Denmark), software which is sed to detect and analyze grains, particles, inclusions and pores (Ref 13). Five LOM micrographs at 100x and five different LOM micrographs at 200x were processed for each set of samples. Interface coating-substrate porosity was not considered.

2.4 Microhardness Analysis

The microhardness measurements on metallographically prepared cross-sections (plate samples: see **Table 3**) were also performed. Using a microhardness tester (VMHTAUTO, Leica, Wetzlar, Germany) starting at the coating surface and reaching the substrate using step size of 50 μm, the Vickers 10 g load indentations were performed inside each coating. The average microhardness and standard deviation of the powder were also reported; more than 20 indentations were performed on a metallographically prepared sample.

2.5 Adhesion and Cohesion Tests

Adhesion and cohesion test were performed following ASTM C633 and the Tubular Coating Tensile test (TCT). A mechanical testing machine (MTS Systems Corporation, Eden Prairie, MN US) under force control was used and the load was measured by a 50 kN load-cell (MTS Systems Corporation). The averages and standard deviations of three (cohesion samples: see **Table 3**) and four (adhesion samples: see **Table 3**) measurements per set were calculated.

2.6 Thermal Analysis

Thermal analysis was performed on adhesion samples during deposition with parameters of **Table 1**. The adhesion samples were drilled on the center of the back side with respect the deposition surface and a temperature k-probe was positioned (embedded in the sample) at 0.5 mm from the deposition surface. The data was recorded by a 17B Fluke digital multimeter (Fluke Corporation, 6920 Seaway Blvd Everett, WA 98203, USA). To reduce the influences of the different gun approach to the sample the data records were started at 60 °C for all measurements.

2.7 Residual Stress Measurement (MLRM)

The Modified Layer Removal Method allows measuring the dimensional deformation of a substrate after subsequent layer removal by mechanical polishing. Automatic grinding (AbraPol-20 Struers Ltd., Mississauga, Canada) was performed using grit-30 abrasive paper for 15-20 s at 75 N with the rotating speed at 150 rpm. The principle of this characterization is based on measurements of substrate displacements induced by removing a small layer of stressed coating. In this work, the related strains along the surface were measured by a Strain Gage (Vishay CEA-125WT-120/350, Vishay Precision Group, Malvern, PA), recorded by means of a Strain Indicator (Vishay Micro-Measurements mod. P3) and converted via software into the relative stresses according to Kroupa and Rybicki (Ref 14, 15). The strain gage was glued on the center of the uncoated side of a sample after cleaning the substrate surface with degreasing agents. Wires were welded onto the terminals and protected with a sealant to avoid exposure (water, etc.). The measurements were performed with respect to two orthogonal directions of the MLRM sample (see **Table 3**): longitudinal and transverse. The average of all the longitudinal and transverse depth profile measurements was taken to characterize the residual stress of the coating. Moreover it was analyzed the variation of average residual stress measures inside subsequent layers of 0.6 mm (thickness) from coating interface up to coating surface; no more depth profile consideration was proposed because they were reported in a previous study (Ref 12).

2.8 Four-point Bending Test

All the four-point bending tests were performed on an MTS mechanical testing machine (MTS Systems Corporation) under force control in a four-point bend rig. The load was measured by a 50 kN load-cell (MTS Systems Corporation). The loading applicator, with convex knives edge (radius 0.003 m), were spaced 0.06 m and 0.04 m apart (respectively: upper and lower applicator). The tests were made in tensile load for the coating (4-point samples: see **Table 3**): the coating was positioned in contact with the larger spacing knives. Bending strengths, σ, were computed from the maximum load P_r that caused the coating to rupture, using the standard relationship (ASTM E855/90):

$$\sigma_r = \frac{3P_r a}{bh^2} \qquad (1)$$

where a is the spacing (normal to load) between upper and lower loading knives, b and h are the specimen width and thickness respectively.

The maximum strain (rupture) ε_r in the limit of small bending is given by:

$$\varepsilon_r = \frac{h\Delta z}{a(L-2a)} \qquad (2)$$

where Δz is the linear displacement (rupture) of the load applicator in the direction of load and L is the larger spacing of upper knives. The elastic modulus was computed from (1) and (2) using Hooke's law. Uncoated strips (2 mm and 4 mm in thickness) were also tested. In this cases, where there wasn't break, and for set 1, where it is difficult to identify coating break point, the load P_r (in order to calculate the bending strength) and the displacement Δz (necessary to calculate the strain) were taken in the upper limit of

linearity (elastic behavior) from load-displacement curve. This upper limit of linearity was calculated by instrument software considering the second derivate of load-displacement curve.

2.9 Fractographic Analysis

To properly interpret mechanical testing results, the measurements of 4-point test and determine the failure dynamics, the characteristics of the fracture surfaces of the cohesion samples after testing were qualitative analyzed by scanning electron microscopy (SEM, model VEGA LMU, TESCAN, Brno, Czech Republic).

3   Results and Discussion

A preliminary consideration is necessary because there are differences in thickness for the different substrates (plate, 4-point and adhesion) obtained by the same cold spray deposition process (**Table 2** and **Table 3**). This discrepancy already noticed in a previous work (Ref 12) is mainly due to a different substrate geometry and heat capacity of the sample holder, which affects the sample temperature during the spray. Higher substrate temperature enhances the deposition efficiency as reported by Kulmala et al. (Ref 16).

3.1 Microstructure and Pore Analysis

The particles are spherical with the presence of some satellites pointed by arrows in SEM micrography of **Fig. 2a**, the particle distributions, reported on **Fig. 2b**, determined by LOM images agree with the powder datasheet provided by the manufacturer. The particle distribution count shows a bimodal trend with two main peak at 9 µm and 22 µm.. The gas atomized particles show a grain microstructure **Fig. 3a**. Aluminium coatings show compact microstructure with the presence of porosity as shown in **Fig. 3b** and **Fig. 4**. The pores are mainly elongated and interstitial as show in **Fig 2b**. In all etched coatings the microstructure shows no noticeable variations as a function of thickness and number of layers in the range investigated: the grain particle microstructure was preserved in the coatings; no recrystallization or grain refinement was noticed. At the interface between the substrate and the coating, the presence of alumina particles used for the grit blasting can be seen in all the samples of **Fig. 4**. The particles aspect ratio (the ratio between the largest diameter and the smallest diameter orthogonal to it) is close to 0.3 - 0.6; some aspect ratio examples are shown in **Fig. 3b**. This indicates that there is a large deformation of AA6061 particles (Ref 17) which is an important feature for high particle cohesion. Porosity analyses were performed on all sets of coating **Fig. 4** and the results are reported in **Fig. 5.** The average porosity and standard deviation show two different trends; the first as function of coating thickness (1 to 4) and the second one as a function of the number of pass (4 to 7). The porosity ranges between 0.3-1.1 % of coating area and it is constant (about 0.3 %), within the statistical error, for the set obtained by a singlepass and varying the coating thickness. The sets from 4 to 7, increasing number of pass and constant coating thickness, exhibit an increase of porosity as a function of the number of passes which is in agreement with a previous work (Ref 12) where it was observed a localized increase in porosity between two subsequent pass.

3.2 Mecchanical Properties

3.2.1 Microhardness Analysis. The Vickers indentation profiles indicate that the microhardness is mainly constant along the coating thickness, so the mean coating microhardness was used in computing the average of the entire dataset. The results are shown in **Fig. 6**, where the averages Vickers hardness of the aluminium alloy coatings are reported as a function of each set. The coatings exhibit a microhardness average of about 100 HV0.01. In comparison, the particles microhardness was 64±8 HV0.01 indicating that the particles are hardened during deposition as reported in other works (Ref 11, 18). The maximum microhardness (105 HV0.01) was obtained with the set 4 (1.9 mm thick, singlepass) and, thought the standard deviation of the measurements is over 15 HV0.01, two trends can be observed, one for the singlepass and different thickness coatings (set 1-4) and one for the multipass coatings (set 4-7). The increase of microhardness as a function of the thickness can be attributed to an increase of peening effect, densification and work hardening of the coating (Ref 19). Conversely, the decrease of microhardness related to the increment in the number of pass can be attributed above all to the lower microhardness measurements in the depth profile localized at the interface between sequential pass as previously explained (Ref 12).

3.2.2 Influence of Heat Gas Flux on Residual Stress Measurement. The MLRM trend (**Fig. 7.a**) shows a residual stress loss in magnitude (mathematical modulus) (set 1-4) from 100 MPa to about 60 MPa with increasing coating thickness. The multipass coating (set 5-7) and for the thicker singlepass coating (set 4) had the compressive residual stresses of about 60 MPa. This behavior is compatible with a stress relieving behavior that is a function of the heated substrate temperature during deposition due to the time of permanence of the hot process gas (bow shock) on the substrate (Ref 20) as previously reported (Ref 12). In order to confirm the stress relieving it was analyzed the stress behavior near the interface between coating and substrate and in the coating surface. In **Fig. 7.b** was reported the average stress measures inside subsequent layers of 0.6 mm (thickness) from coating interface up to coating surface. The compressive residual stress near the interface decreases, up to 30 MPa with the increase of coating thickness independently of the number of passes; contrarily the residual stress in the coating surface remains constant: about 90 MPa for all set. The coating interface, with respect to coating surface, had a prolonged time of exposure to the cold spray heat gas flux (Ref 20) giving rise to the higher stress reliving. The sample temperature measured in function of deposition time is reported on **Fig. 8**. For the singlepass coatings: set 1, 2, 3 and 4, the exposure time to a temperature greater than 60°C to a maximum of about 190°C, was respectively 120, 170, 260 and 480 s, while for the multipass coating: set 5, 6 and 7, the exposure time was the same of about 490 s. Other considerations on temperature coming from the analysis of graphics of **Fig. 8** must be reported. The gun movement following the Zig-Zag pattern induced a double variation of temperature on each point of the sample. The first variation is due to the hot gas flux that runs over and out the sample for each scan (see **Fig. 1**), rising and lowering the temperature. The second variation of temperature, present only in the multipass depositions, is due to repetition of the whole Zig-Zag pattern. As it can see on **Fig. 8**, the amplitude of first variation of temperature was reduced increasing the gun speed (**Table 2**). More, for each variation due to the multipass deposition, the maximum temperature of each pass rise down consequently to the increase of coating thickness (increase of the thickness of AA6061 material between k-probe and heat gas flux). Taken in account these two variations, the average temperature, calculated during the spray time (temperature over 60 °C), was the same for all coatings at 145.9±7.4 °C.

The peening effect, above all, of grit blasting particle impacts on substrate surface, was also measured by MLRM: the measured compressive stress in the layers of 0.6 mm (thickness) from interface, ranges from 31 MPa (set 3) up to 85 (set 6) MPa, but no trend was found. The MLRM investigation was stopped at a substrate depth equal to 2 mm, in this last substrate layer (from 0. 6 mm to 2

mm) a tensile stress of about 139 ± 28 MPa was measured independently from deposition strategy. This tensile stress in the coating is a typical substrate stress compensation of peening effect.

3.2.3 Influence of Residual Stress on Coating Adhesion. All the adhesion samples tested exhibits an adhesion failure at the substrate-coating interface: no cohesion failure is observed. Similar to previous observations, there are distinct trends for the singlepass and multipass coatings (**Fig. 9**). In the range examined for the singlepass coating adhesion to the substrates appear not to be affected by coating thickness and the adhesion strength is constant at 33 MPa. Increasing the number of passes negatively affects the coating adhesion. The singlepass with a 2.5 mm thickness had adhesion strength of 31 MPa while the 4-pass coating with 2.5 mm thickness dropped to 21 MPa. Although there may be a correlation between stress relieving on the coating interface and particle-substrate interlocking, that relates the stress measurements (**Fig. 7**) with the adhesion results (**Fig. 9**), it is clear there be other causes affecting the adhesion that directly involves the increase of layers. In fact the stress relieving at the interface could loosen the mechanical adhesion between the particles interlocked in the substrate; however the stress behavior was shown to be correlated with the coating thickness, not numbers of layers as it was found in the results of adhesion. Another result coming from stress analysis, reported in a previous study (Ref 12), highlighted the presences of tensile peaks (150 MPa) at the layers interface, although it's not yet understood the mechanism by with the increase of passes affected negatively the adhesion, the presences of these tensile peaks in the coating could play a role in the coating adhesion failure. More targeted investigations are ongoing.

3.2.4 Valuation of Deposition Strategies by Tensile (TCT) and Bending (Four-point) Tests. Results of the cohesion (TCT) analysis were quite different from previous observations: there was no evidence of any particular trends as a function of thickness nor as a function of the number of pass as can be seen in **Fig. 9**. Only the first set (1), which thickness of 0.6 mm exhibited a little higher cohesion strength than the other sets. Ultimately the cohesive strength for all the sets was relatively constant at about 80 MPa for all thicknesses and the number of layers. The multilayer strategy of deposition didn't affect the cohesion results, in this case the tensile load of cohesion test acted parallel (shear force) to the subsequent layers interfaces without any appreciable influence on coating cohesion. In order to evaluate and to understand the behavior of the mechanical properties: ultimate strength (rupture) and modulus when the tensile load was applied perpendicular to interface layers, it was performed the four-point bending test with according to the geometrical parameters of deposition (Zig-Zag pattern) of **Fig. 1.b**.

The load-extension chart of **Fig. 10** presents a representative measurements obtained from the four-point bending test that evaluated the seven sets and the blank substrates (thickness: 2 and 4 mm). The blank AA6061-O samples exhibit elastic and plastic behavior. The samples of set 1 also show elastic and plastic behavior although there were several cracks in the coating (**Fig. 10c**). There is no appreciable indication of their influence on the load or extension measurements. Set 2, for a load greater than 1 kN exhibit two successive breaks: the first at an extension of 0.6 mm and the second at 0.8 mm. The two respective transverse cracks on the coatings appeared at applied loads at the knives. The measurements after the breaks proceeded without an increase in load until the extension reaches 2 mm, at this stage the coating delaminated from the substrate. All the cracks reported were transverse, that is parallel to samples width (**Fig. 10c**) and, referring to **Fig. 1b**, perpendicular to gun movement during spraying. The pattern of deposition, in particular the spray direction, could have large influence on the bending test. It was chosen the pattern of **Fig. 1b** instead the spray direction perpendicular to long axis of 4-point strip to avoid the possibility of the transverse crack to propagate through the coating parallel to scan deposition. It was tested that the strategy of deposition with spray direction parallel to 4-point strip dramatically

reduces the rupture-load P_r. As an example, not being covered other strategies of deposition in this study, the rupture-load of the 2 mm singlepass coating was 17 MPa, 55% lower than the correspondent sample deposited with a spray direction perpendicular to the strip.

After a complete detachment of the coating between the two cracks, the load-extension curve advances following the same plastic trend of blank samples. The other set (3, 4, 5, 6 and 7) showed the same load-extension trend described for set 2, however the first break was much more evident and easy to identify in the curve. In the chart load-extension (in **Fig. 10a**) for the set 3, 4, 5, 6 and 7, the data reported is up to the second break; the magnification of these curves (up to the first crack) is reported in **Fig. 10b**.

The elastic modulus of samples of the seven sets and blank strips were also calculated following formulas (1) and (2). The results (average and standard deviation) and the relative loads at break (average and standard deviation) are reported in the histogram chart of **Fig. 11**. The load at break, as expected, increases as the coating thickness increases (set 1 to 4). In the case of comparison of number of layers (set 4 to 7 with the equal thickness) large a difference is noticeable between single and multilayers coatings: the coatings deposited by 2, 3 and 4 pass show similar load at break (2.4-2.5 kN) that is 14-19 % higher than the load at break (2.1 kN) reported for singlepass coating.

The bending elastic modulus (**Fig. 11**) calculated for the blank AA6061-O laminated strips is 96.6±3.3 GPa and 91.5±0.3 GPa (respectively 2 mm and 4 mm blank strips), higher than the well known modulus measured in tension, 60-70, GPa (Ref 21). The discrepancy between the measurements in bending (three- or four-point) and in tension is well known and reported by Berthelot et al. (Ref 22). The modulus value, maximum for the blank samples, decreases in sets 1 to 4 with increases in deposit thickness (on the same thickness substrate). The elastic modulus increases for each added layer in function of the number of layers.

The 4-point bending test performed on strip with coating, measures the mechanical properties of the whole samples (strip plus coating), these measurements are quite interesting to understand the interaction of the coating on bulk material. It's also important to understand the mechanical behavior of the coating without the influence of strip. The modulus of the *freestanding* coating (coating without strip) can be evaluated by linear regression considering the behavior of elastic modulus of the samples where the coating thicknesses grow with respect to the constant thickness of the strips, that is, the sets 1, 2, 3 and 4. Before, some considerations are necessary. The 4-point bending test acts on samples (with or without coating) applying both tensile than compressive load. The tensile load is applied on the top side of sample (upper knives) and the compressive load on the bottom side of sample (lower knives). From this consideration, the coatings of sets 1, 2 and 3 in the bending test were subjected only to a tensile load, while the thicker coatings of sets 4, 5, 6 and 7 were loaded principally under tension, however there was a compressive load in the thin layer from the coating-substrate interface up to the middle of sample thickness (strip plus coating), see the right-upper layout of **Fig. 12.a**. In the same manner, the 2 mm strips, the substrate of all the coatings, are subjected to tensile and compressive load for set 1, 2 and 3 and only compressive load for the samples of set 4, 5, 6 and 7. Another consideration must take in account. For bulk material, compressive and tensile tests give the same Young modulus, only the presences of defects like porosity or void can reduce the results measured in tensile with respect compressive test, this because the pore and the void may open easily on tensile load. This is not the case of AA6061 coatings, in fact examining the increase of porosity reported for the multilayer coatings, **Fig. 5**, and comparing with the modulus reported in the histogram of **Fig. 11**, it is observed an increase in the modulus as the number of layers grows.

All these considerations validate the possibility to evaluate, by linear regression, the elastic modulus of freestanding coating analyzing the set 1, 2, 3, and 4. In **Fig. 12a** the elastic modulus in function of sample ratio: strip and coating section (A) divided by coating section (A_c) shows that the elastic modulus is linear dependent on this ratio (quadratic correlation coefficient: 0.9985). In the linear regression the influence of substrate decreases with increasing coating thickness and when the ratio A/A_c is equal to 1 the thickness of the coating is equal to the thickness of the whole sample and the strip thickness is equal to zero. In this case (lim $A/A_c=1$ for $A \rightarrow A_c$) the elastic modulus reported in the graphic of **Fig. 12a**, 38 MPa, is the elastic modulus of the freestanding coating of singlepass coatings of set 1, 2, 3 and 4. Vice versa the influence of substrate is easily determined subtracting the obtained elastic modulus of freestanding (singlepass) coating to the elastic modulus of each sample (coating plus strip) for each set of the linear regression.

Remembering that the modulus of the multipass coatings of set 4, 5, 6 and 7 grows with the increase of number of layers **Fig 11** and remembering that all set (4, 5, 6, and 7) have the same thickness, it's easily estimated the elastic modulus of freestanding coatings of multipass set by removing the substrate influence derived from linear regression (set 4) of singlepass coatings. The freestanding modulus of multipass coatings is presented in **Fig. 12b**, where is also reported the percentage of modulus with respect the bulk material (4 mm blank sample). The evaluation of singlepass coating with respect multipass coating and bulk material (**Fig. 12b**) shows that the elastic moduli of cold spray freestanding coatings increase from 38 GPa (set 1, 2,3, and 4) up to 58 GPa (4 layers: set 7), 63% lower in comparison with 92 GPa of 4 mm blank sample modulus. This modulus behavior could be understood analyzing the different mechanism of fracture of each coating.

3.3 Failure Analysis

The fractures analyzed on deposits of set 1 to 4 (singlepass, different thickness) did not reveal any differences: the fractures are homogenous as presented in the representative micrograph of **Fig 13a**. The coatings of set 5 (two pass coating) show a fracture with the presence of two typology of cracks, one perpendicular to the substrate (pointed by white arrows of **Fig. 13b**), the other parallel to the substrate (pointed by black arrow). The perpendicular cracks propagated (geometrically) from the coating surface to the substrate, stopping at the middle of the deposit, close to the interface of two adjacent layers. From there, the second parallel cracks started and continued until intersecting a new perpendicular cracks which, from this point, propagated to the substrate. Similar behavior was noticed in other multilayer deposit (**Figs. 13c** and **13d**); where the perpendicular cracks come from surface or layer interface to the adjacent layer interface (or substrate); meanwhile the parallel cracks follows the layer interfaces. The failure analysis shows after initiation, a crack propagates until it encounters a discontinuity in the coating such as the interface of next layer. In some cases the interface stops the crack propagation (example in **Figs. 13c** and **13d**), in other cases, the crack continued along the interface. In both cases, respectively, additional energy is required to stretch *bridging* metal layer, as reported by Evans et al. Ref 23 and to fracture a *constraint* layer (Watanabe et al. Ref 24). These failure mechanisms are represented in the schematic of **Fig. 14** differentiating in singlepass coating **Fig. 14a** and multipass coating **Fig. 14b**.

The surfaces examined at higher magnifications showed mainly a brittle interparticle fracture (**Fig. 15a**), however ductile fractures are observed in the highly deformed particles in the dimples as shown in **Fig. 15b**.

4   Summary and Conclusions

AA6061 aluminium alloy powder was deposited by cold spray on AA6061-O substrate in order to perform the metallographic, the mechanical and the fractographic analysis. Seven coating sets were produced for each type of characterization. The coating for sets 1 to 4 were deposited in a singlepass varying the coating thickness, the coating for sets 4 to 7 were applied using multiples passes to a constant overall coating thickness.

The metallographic examination on cross-section coatings shows highly deformed particles for all sets. Porosity analysis shows very low pore content in singlepass coating and a slight increase in porosity as the number of coating layers is increased. It was observed that the increase of porosity is localized between two subsequent pass in the multilayer coatings.

The depth profile microhardness shows a hardening (about 50 %) of the coating with respect to the gas atomized particles. Although each average measurement is inside the standard deviation, the coating microhardness seems to increase with the increasing of thickness and to decrease with the number of layers. These behaviors can be attributed respectively to an increase of peening effect, densification and work hardening of the coating (Ref 19) and to the lower microhardness measurements in the depth profile localized at the interface between sequential pass (Ref 12).

The compressive residual stress measurements performed by MLRM are stable at -60 MPa for the thicker coating independent of the number of passes while, the compressive stress is greater (mathematical modulus) in the low thickness coating. In the depth profile analysis it was noticed that the coating surface was about -90 MPa for each set, meanwhile near the substrate-coating interface the compressive stress intensity lowered with increasing the coating thickness independently of number of passes (about -30 MPa for the set 4, 5, 6 and 7). This behavior is mainly attributed to thermal stresses reliving in proportion to exposure time of heat gas flux during the deposition.

The mechanical study on the coating following ASTM C633 and TCT test reveals that the cohesion strength was approximately 80 MPa for all sets. The tensile traction of cohesion test acted parallel (shear force) to the subsequent layers interfaces of the coated cylindrical samples without any appreciable influence on coating cohesion, so the multilayer strategy of deposition didn't affect the cohesion results.

Adhesion test results revealed the two trends highlighted by metallographic analysis: a constant value (more than 30 MPa) is observed for the singlelayer coating independently of coating thickness and a decrease in adhesion strength (from 31 MPa down to 20 MPa) is observed as a function of the number of passes. The variation of adhesion in function of number of layers is not yet understood.

The four-point bending test shows an elastic modulus reduction with an increase in coating thickness deposited in a singlepass on 2 mm-thick strips. A linear regression analysis of these samples shows that for freestanding cold spray coatings (coating without substrate) the elastic modulus is 38 GPa, 42% lower with respect to the modulus of AA6061-O laminated strip (92 GPa). Quite interestingly, an increase of modulus is observed for each added layer in the multipass coatings, up to 58 GPa of four-pass coating, 63% lower with respect to the blank sample. This behavior is similar to laminate composite behavior (Ref 25) and is explained by

fractographic analysis, where a crack stopping and energy dissipation are localized on interface between next layers. All the data is summarized in **Table 4**

The AA6061cold spray coatings deposited by the two different strategies of deposition: single and multilayers show different mechanical properties in the range of presented investigations. The singlelayer coating exhibits more compact coating with less porosity. The multilayer coatings don't present uniformity in all the coating section, the discontinuity between layers is highlighted by an intensification of porosity in the layers interface. Not only morphological differences, but also the mechanical properties vary in the layers interfaces. In fact, in a previous and preliminary study (Ref 12) was noticed a tensile residual peak and a lower microhardness localized between two subsequent layers. These discontinuities don't influence the cohesion of the coating measured by TCT, this because the tensile load of the test acts parallel to the interface layers in the coated cylindrical samples. Moreover the discontinuity of the multilayers confers properties, such as of the laminate composite, increasing the elastic modulus in function of number of layers when tested by four-point. Indeed, in this test, the load was applied, moreover, perpendicularly to the layer interfaces.

The multipass strategy affects negatively above all the coating adhesion. However it has been hypothesized a correlation with tensile stress peaks at the layers interfaces, no direct connection were noticed. More targeted investigations are ongoing.

Finally the examination of depth residual stress analysis shows that there is a stress reliving near coating-substrate interface, greater, the greater is the coating thickness independently by the number of pass. This was attributed to thermal reliving proportionally to the time of permanence of heat gas flux of cold spray on the sample.

The study highlights the importance of the choice of the cold spray strategy of deposition on the coating final properties, pointing out that the geometrical parameters of deposition play a role in the coating quality in function of the typology of stress that the restored component is subject or in function of desired requirement. Other geometrical variations of the deposition pattern (for example crossed zig-zag in multipass coating) could be considered to obtain desiderated quality in the component restorations.

Acknowledgements

5   References

1.   Victor K. Champagne, The Repair Of Magnesium Rotorcraft Components by Cold Spray, J. Fail. Anal. and Preven. 2008, 8, p 164–175.

2.   Q. C. Liu, P. Baburamani, W. Zhuang, D. Gerrard, B. Hinton, M. Janardhana and K. Sharp, Surface Modification and Repair For Aircraft Life Enhancement and Structural Restoration, Materials Science Forum, 2010, 654-656, p 763-766.

3.   J.C. Lee, H.J. Kang, W.S. Chu and S.H. Ahn, Repair Of Damaged Mold Surface by Cold-Spray Method, CIRP Annals - Manufacturing Technology, 2007, 56, (1), p 577-580.

4. Efforts to Reduce Corrosion on the Military Equipment and Infrastructure of the Department of Defense, Department of Defense Report, Office of the Secretary of Defense, June 2007.

5. P. Fauchais and G. Montavon, Thermal and Cold Spray: Recent Developments, Key Engineering Materials, 2008, 384, p 1-59

6. S. Katsas, J. Nikolaou and G. Papadimitriou, Microstructural Changes Accompanying Repair Welding in 5xxx Aluminium Alloys and Their Effect on the Mechanical Properties, Mater. Des., 2006, 27, p 968–975.

7. S. Ignata, P. Sallamandb, D. Greveyb and M. Lambertina, Magnesium Alloys Laser (Nd:YAG) Cladding and Alloying with Side Injection of Aluminium Powder, Applied Surface Science, 2004, 225, p 124–134.

8. R. Song, S. Hanaki, M. Yamashita and H. Uchida, Reliability Evaluation of a Laser Repaired Die-Casting Die, Materials Science and Engineering, 2008, A 483–484, p 343–345.

9. K. Shankar and W. Wu, Effect of Welding and Weld Repair on Crack Propagation Behaviour in Aluminium Alloy 5083 Plates, Mater. Des., 2002, 23, p 201-208.

10. S. Rech, A. Trentin, S. Vezzù, E. Irissou, J. G. Legoux, B. Arsenault, M. Lamontagne, C. Moreau and M. Guagliano, Characterization of Residual Stresses in Al And Al/Al2O3 Cold Sprayed Coatings, International Thermal Spray Conference & Exposition 2009, Ed., May 4-7, 2009, Las Vegas, Nevada, ASM International, 2009, p 1012-1017.

11. A. Papyrin, V. Kosarev, S. Klinkov, A. Alkhimov and V. M. Fomin, Chapter 4—Cold Spray Equipments and Technologies, Cold Spray Technology, 1st ed., Elsevier Ltd, Amsterdam, 2007, p 179-247

12. S. Rech, J.G. Legoux, E. Irissou, A. Trentin, S. Vezzù and M. Guagliano, Influence of Pre-Heated Al6061 Substrate Temperature on the Residual Stresses Of Multipass Al-Coating Deposited By Cold Spray, J. Therm. Spray Technol., 2011, 20 (1), p 243-251.

13. Particle & Pore Analysis Module in SPIP, Image Metrology, http://www.imagemet.com.

14. F. Kroupa, Residual Stresses in Thick, Non-Homogenous Coating, J. Therm. Spray Technol., 1997, 6 (3), p 147-150.

15. E. F. Rybicki, R. T. R. McGrann, and J. R. Shadley, Applications and Theory of The Modified Layer Removal Method for the Evaluation of Through-Thickness Residual Stresses In Thermal Spray Coated Materials, In The Fifth Int. Conf. Residual Stresses, ICRS-5, Linköping, 1997, p 994-999.

16. M. Kulmala and P. Vuoristo, Influence of Process Conditions in Laser-Assisted Low-Pressure Cold Spraying, Surf. Coat. Technol., 2008, 202, p 4503–4508.

17. T. Schmidt, F. Gartner, H. Assadi and H. Kreye, Development of a Generalized Parameter Cold Spray Deposition, Acta Mater., 2006, 54, p 729-742.

18. S. Gulizia, A. Trentin, S. Vezzù. S. Rech, P. King, M. Jahedi and M. Guagliano, Characterisation of Cold Spray Titanium Coatings, Materials Science Forum, 2010, 654-656, p 898-901.

19. T.H. Van Steenkiste, J.R. Smith and R.E. Teets, Aluminum Coatings Via Kinetic Spray with Relatively Large Powder Particles, Surf. Coat. Technol., 2002, 154, p 237–252.

20. A.G. McDonald, A.N. Ryabinin, E. Irissou and J.-G. Legoux, Gas-Substrate Heat Exchange During Cold-Gas Dynamic Spraying, J. Therm. Spray Technol., 2013, 22 (2-3), p 391-397.

21. Properties and Selection: Non Ferrous Material, Aluminum Mill and Engineered Wrought Products, ASM Handbook, Edition Metals Handbook, 1990, 2, p 118-222.

22. J. M. Berthelot and L. Fatmi, Statistical Investigation of The Fracture Behavior of Inhomogeneous Materials in Tension and Three-Point Bending, Engineering Fracture Mechanics, 2004, 71, p 1535–1556.

23. A.G. Evans and R.M. McMeeking, On the Toughening of Ceramics by Strong Reinforcements, Acta Metall. 1986, 34, p 2435–2441.

24. M. Watanabe, M. Komatsu and S. Kuroda, Multilayered WC–Co/Cu Coatings by Warm Spray Deposition, Surf. and Coat. Technol., 2011, 205, 23–24, p 5358-5368.

25. Fatigue and Fracture, Fatigue of Composite Laminates, ASM Handbook, Edition Metals Handbook, 1990, 19, p 2324-2363.

Table 1: Aluminium Alloy 6061 powder composition.

Element	%wt
Silicon	0.63
Iron	0.42
Copper	0.22
Manganese	0.09
Magnesium	1.00
Chromium	0.31
Zinc	0.18
Titanium	0.09
Other	0.12
Aluminium	remainder
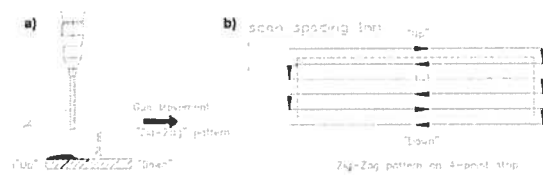
Fig. 1: (a) nozzle-substrate relative angle and stand off-distance. (b) Zig-Zag pattern of deposition on substrate (in particular: 4-point strip).

Table 2: main deposition parameters.

Spray parameter	Plate, 4-point, Adhesion, MLRM (samples)	Cohesion (sample)
Gas temp.	350 C°	350 C°
Gas press.	3.1 MPa	3.1 MPa
Standoff dist.	20 mm	20 mm
Scan spacing	1 mm	1 mm (estimated)
Scan speed	24-12-8-6 mm/s	0.4-0.3-0.2-0.1 mm/s
Sample rotation	-	22-18-12-6 RPM
No. pass	1 to 4	1 to 4

Table 3: the coating thickness (mm) of the entire set of samples obtained by cold spray deposition of AA6061 powder on AA6061 substrates.

Sample	Set 1	Set 2	Set 3	Set 4	Set 5	Set 6	Set 7
Plate	0.50±0.06	1.04±0.11	1.51±0.09	1.87±0.07	2.01±0.15	2.12±0.15	2.05±0.16

4-point	0.58±0.05	1.19±0.04	1.80±0.08	2.47±0.01	2.40±0.08	2.51±0.01	2.49±0.05
Adhesion	0.64±0.06	1.26±0.05	1.77±0.05	2.48±0.05	2.50±0.09	2.46±0.12	2.52±0.14
Cohesion	0.60±0.03	0.79±0.02	1.15±0.01	2.11±0.10	2.13±0.01	2.15±0.04	2.06±0.03
MLRM	0.65±0.18	1.24±0.10	1.73±0.08	2.15±0.09	2.32±0.20	2.55±0.10	2.56±0.08
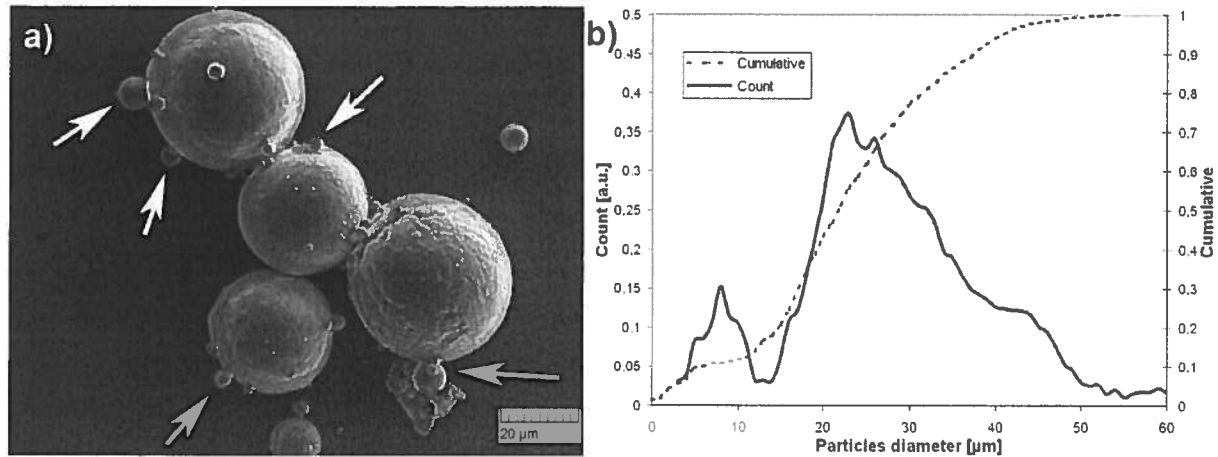
Fig. 2: (a) SEM micrographs of AA6061 aluminium alloy powder: spherical particles with the presence of satellites (pointed by arrows). (b) Distribution of particle diameter of AA6061 powder.
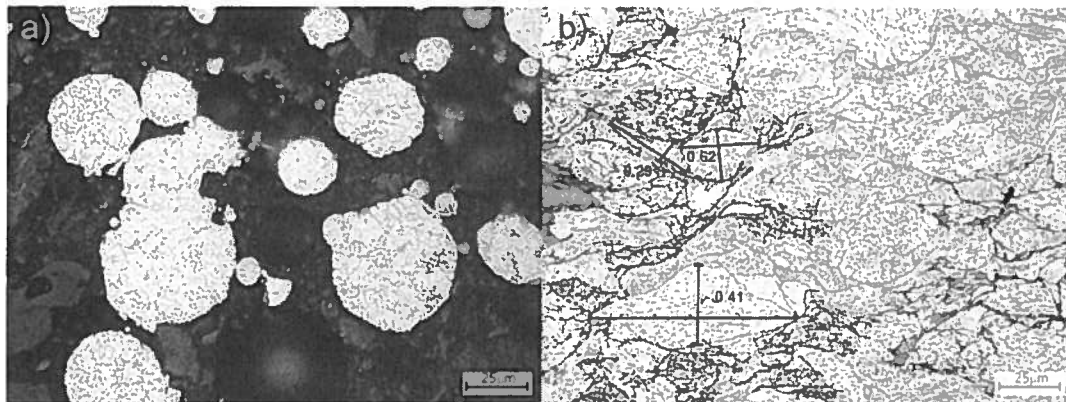
Fig. 3: LOM micrographies of AA6061 aluminium alloy powder and AA6061 coating (set 6) etched by modified Keller's reagent. (a) gas atomized powder. (b) microstructure of coating.
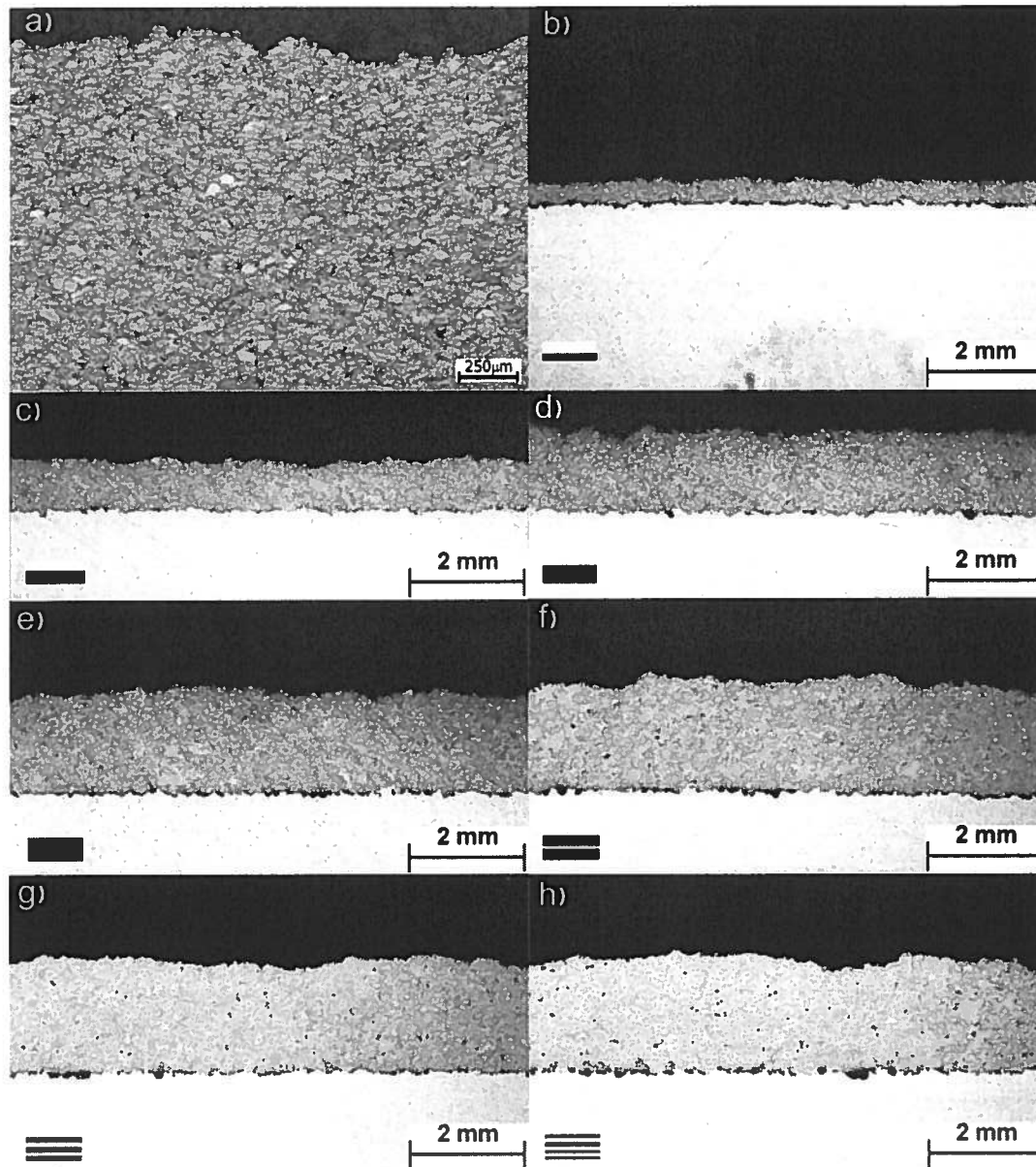
Fig. 4: LOM micrographies AA6061 coating etched by modified Keller's reagent. (a) compact microstructure of coating (set 6). (b-c-d-e) singlepass and different thickness coating: respectively set 1, 2, 3 and 4. (f-g-h) multipass coating respectively set 5, 6 and 7.
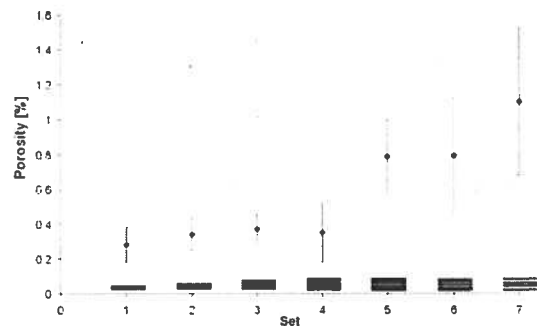
Fig. 5: The average coating porosity and standard deviation obtained by images analysis.
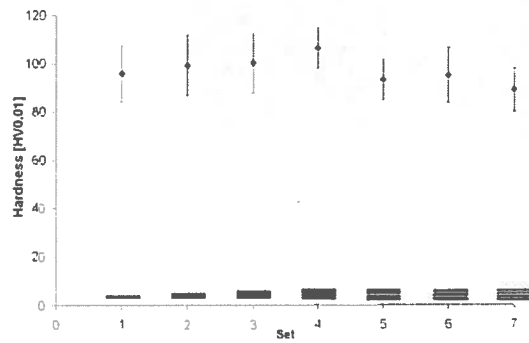
Fig. 6: Average coatings microhardness obtained by depth profile measurements and its standard deviation. The microhardness of powder is 64±8 HV0.01.
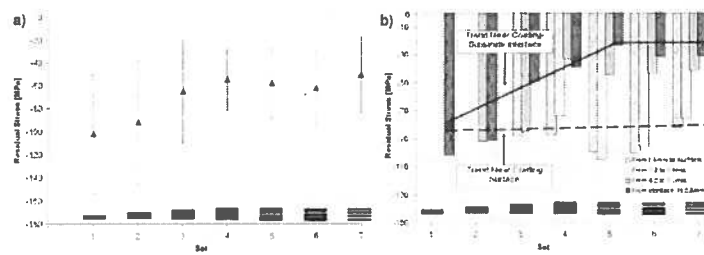
Fig. 7: Residual stresses obtained by depth profile measurements performed by MLRM. (a) average coating residual stress. (b) average residual stress measures inside subsequent layers of 0.6 mm (thickness) from coating interface up to coating surface.
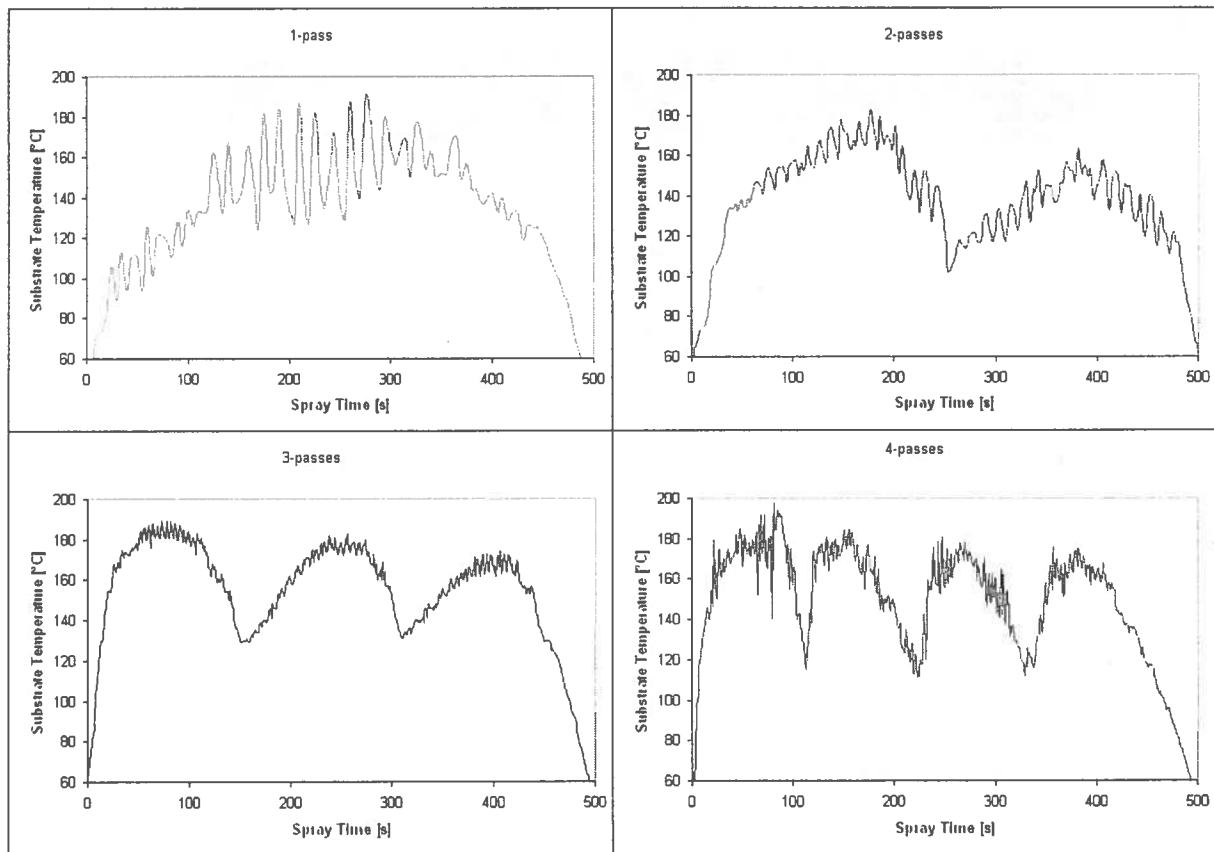
Fig. 8: thermal analysis of cold spray deposition on adhesion substrates. (a) singlepass (set 4); (b) 2-passes (set 5); (c) 3-passes (set 6) and (d) 4-passes (set 7).
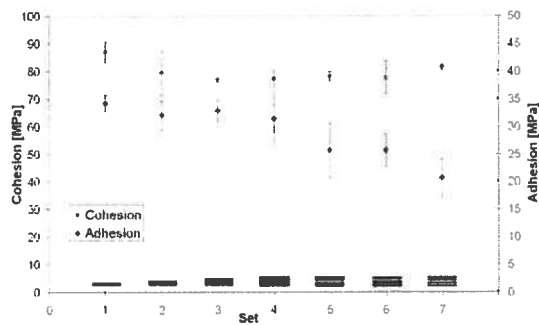
Fig . 9: Adhesion and cohesion measurements following the norm ASTM C633 and TCT test.
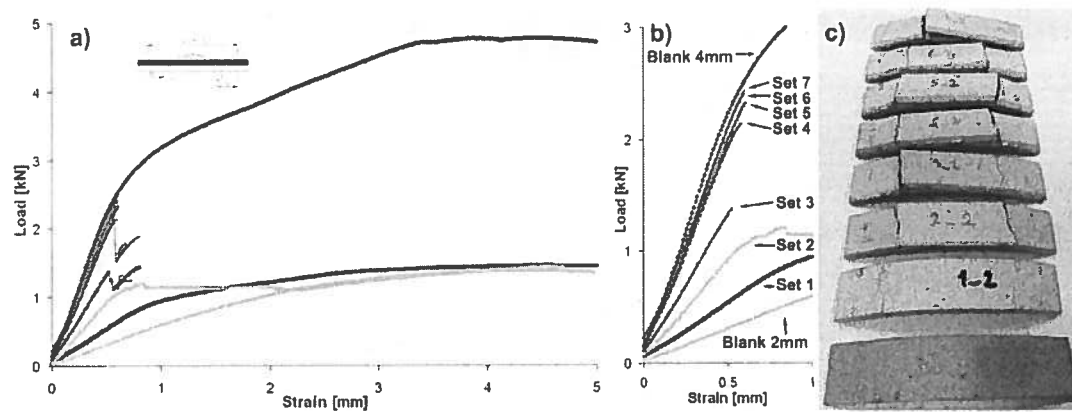

Fig. 10: (a) load-extension chart, reported first and second coating crack. (b) load-extension chart (magnification), only first crack reported. (c) the samples after 4-point test. The apparatus was configured like in the schematic picture (right-top): L=60 mm, a=10 mm and R=3 mm.
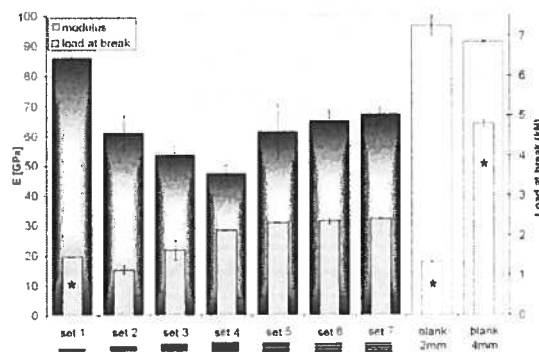

Fig. 11: In the histogram are shown the average load at break and the calculated elastic modulus. The errors reported are the standard deviations. The symbol (*) indicated that the break-load point (also displacement point) were taken in the upper limit of linearity (elastic behavior) from load-displacement data.
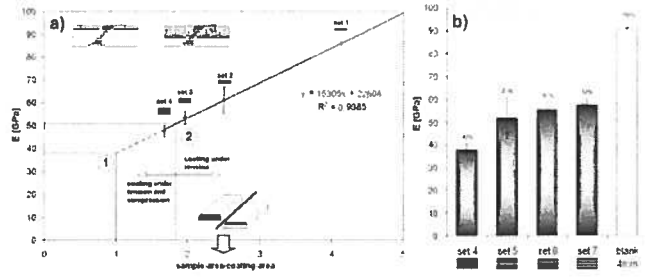
Fig. 12: (a) Linear regression of elastic modulus in function of sample ratio: strip+coating section divided by coating section. Point (1) evaluation of freestanding coating modulus. Point (2) limit between coating work-load: under tension and under tension and compression. (b) elastic modulus calculated by regression of freestanding coatings compared to elastic modulus of 4 mm strip (blank sample).
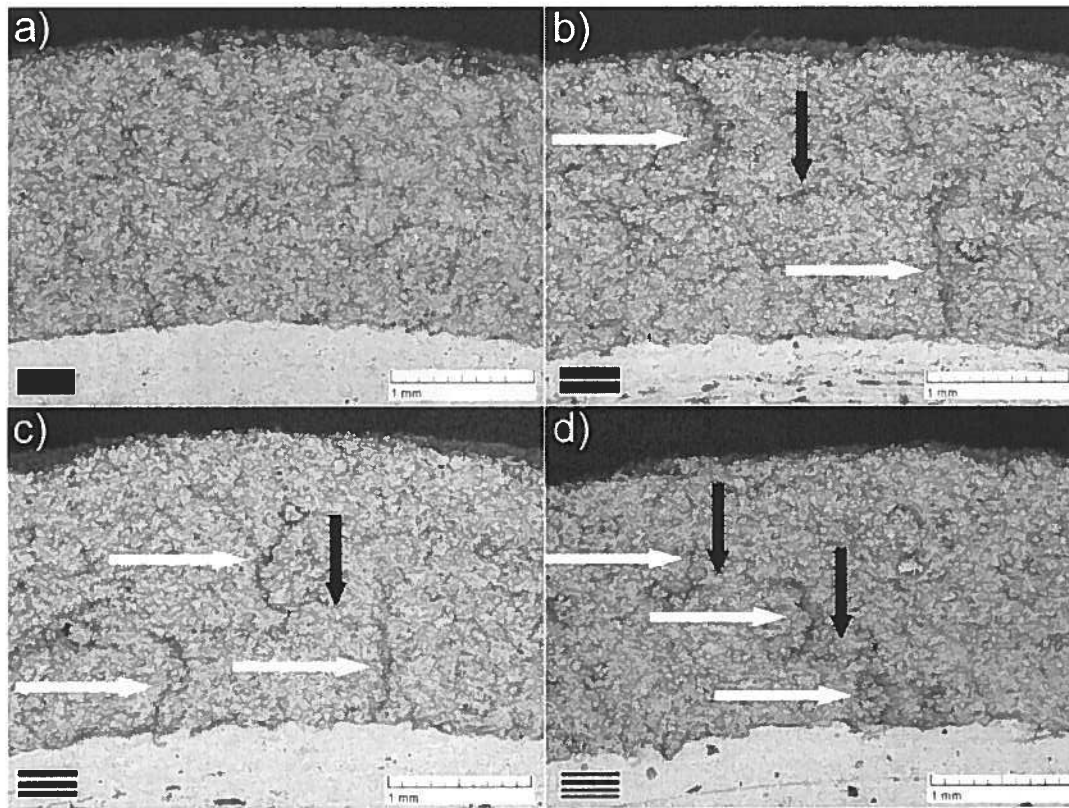

Fig. 13: SEM micrographies of AA6061 coatings fractures. (a) homogenous fracture. (b-c-d) evidence of interlayers cracks (black arrows) and crack propagation between layers (white arrows).
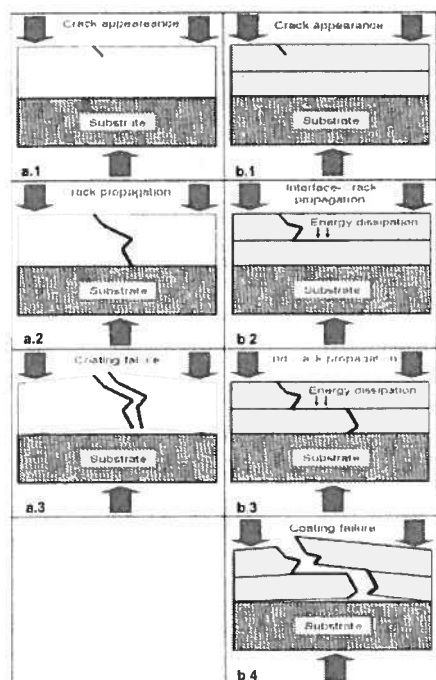
Fig. 14: (a) schematic singlepass coating failure. (b) schematic multipass coating failure.
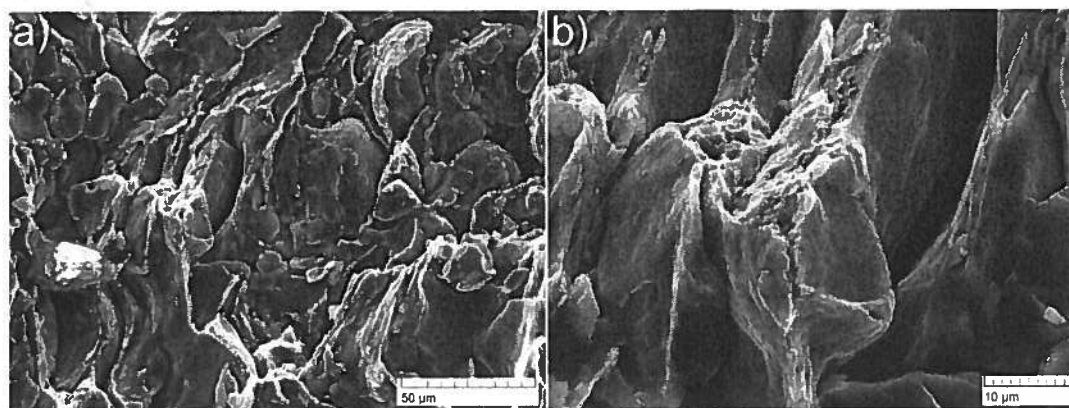

Fig. 15: (a) interparticle brittle fractures and (b) dimpled appearance of ductile particle fracture.

Table 4: Mechanical Coating Properties trends in function of thickness and number of pass.

Property-Test	Growing Thickness		Growing Number of Pass	
Porosity (Image analysis)	→	<0.4%, stable	↑	<1.2%. Grows with the number of layers
Vickers Microhardness	↑	[95-105 HV0.01] Moderate grows with the coating thickness	↓	[105-90 HV0.01] Moderate decreases with the number of layers
Compressive Stress (MLRM)	↓	(Intensity) [100-60 MPa] decreases with the coating thickness	→	(Intensity) ~60 MPa, stable
Cohesion (TCT)	→	~80 MPa, stable	→	~80 MPa, stable
Adhesion (ASTM C633)	→	~33 MPa, stable	↓	[31-20 MPa] Decreases with the number of layers
4-point bending	→	Elastic Modulus of freestanding coating stable	↑	Load at Break and Elastic Modulus grow with the number of layers